Letter

Laser cooling and hyperfine measurements of $^{225}Ra^{+}$ ions

Roy A. Ready,[1,*] Haoran Li,[1] Spencer Kofford,[1] Robert Kwapisz,[1] Huaxu Dan,[1] Akshay Sawhney,[1] Mingyu Fan,[1] Craig Holliman,[1] Xiaoyang Shi,[1] Luka Sever-Walter,[1] A. N. Gaiser,[2,3] J. R. Griswold,[4] and Andrew M. Jayich[1]

[1]*Department of Physics, University of California, Santa Barbara, Santa Barbara, California 93106, USA*
[2]*Department of Chemistry, Michigan State University, East Lansing, Michigan 48824, USA*
[3]*Facility for Rare Isotope Beams, Michigan State University, East Lansing, Michigan 48824, USA*
[4]*Radioisotope Science and Technology Division, Oak Ridge National Laboratory, Oak Ridge, Tennessee 37830, USA*

(Received 19 July 2024; revised 23 September 2025; accepted 26 May 2026; published 7 July 2026)

$^{225}Ra^{+}$ ions (nuclear spin $I = 1/2$) have transitions that are first-order insensitive to magnetic field noise, which is advantageous for optical clocks and quantum information science. We report on laser cooling and trapping of $^{225}Ra^{+}$ ions and hyperfine splitting measurements of the ion's $7s\,^2S_{1/2}$, $7p\,^2P_{1/2}$, and $6d\,^2D_{3/2}$ states. We measured the ground-state hyperfine constant, $A(S_{1/2}) = -27.684\,511\,052(5)$ GHz, and the quadratic Zeeman coefficient, $C_2 = 142.3(1.0)$ Hz G^{-2}, of the $^2S_{1/2}(F = 0, m_F = 0) \leftrightarrow {}^2S_{1/2}(F = 1, m_F = 0)$ transition. Our result addresses a discrepancy in the literature for the ground-state hyperfine splitting. We measured the hyperfine constants of the $^2P_{1/2}$ state, $A(P_{1/2}) = -5.447(4)$ GHz, and the $^2D_{3/2}$ state, $A(D_{3/2}) = -619.7(1.1)$ MHz. We also performed state preparation and measurement using the ground-state hyperfine levels and realized a fidelity of 0.9951(9).

DOI: 10.1103/krnz-tfh1

Atoms with magnetic field-insensitive transitions are appealing for quantum information science (QIS) [1] and precision measurements [2,3]. For alkalilike ions with a single unpaired electron and half-integer nuclear spin, there is a ground-state qubit composed of two spin projection $m_F = 0$ states separated by the hyperfine splitting. These states are first-order insensitive to magnetic field noise and are well suited to laser-driven gates [4,5]. For laser-coolable ions with nuclear spin $I = 1/2$, the qubit is straightforward to initialize and control optically or with microwaves. Such a hyperfine qubit is a feature of $^{171}Yb^{+}$ [6,7] and $^{133}Ba^{+}$ [8]. These qubit features also benefit optical clocks [9,10]. The $^{225}Ra^{+}$ ion ($I = 1/2$) is a good clock candidate [11], due in part to its low charge-to-mass ratio and optical transitions at convenient wavelengths [12,13]. The ion's large hyperfine splittings make it possible to operate an optical clock with only two infrared wavelengths (828 nm and 1079 nm) [14], which could be generated and controlled with integrated photonics to help enable a compact transportable system.

In this Letter, we report spectroscopy results with single trapped and laser-cooled $^{225}Ra^{+}$ ions. We improve the precision of $^2S_{1/2}$ and $^2P_{1/2}$ hyperfine splittings and realize the first $^2D_{3/2}$ hyperfine splitting measurement. We also characterized state preparation and measurement (SPAM) of the hyperfine qubit using the $S_{1/2} \leftrightarrow P_{1/2}$ and $D_{3/2} \leftrightarrow P_{1/2}$ transitions, demonstrating straightforward, high fidelity control.

Radium is famous for its radioactivity and ^{225}Ra is no exception, with only a 15 d half-life. Despite this apparent obstacle, we have worked with laser-cooled $^{225}Ra^{+}$ ions in a sealed vacuum system since June 6th, 2023. The key to seamless operation is the oven design based on Fan *et al.* [15]. We applied the same technique to thorium-229 (7800-yr half-life [16]), which continuously produces radium via nuclear decay. The ^{225}Ra source is a molecular beam epitaxy oven with 8μCI of ^{229}Th deposited in a titanium crucible [15], which generates 3×10^{11} atoms over one ^{225}Ra half-life. The oven is heated to between 350 and 500 °C to effuse radium atoms, see Fig. 1(b). Radium ions are loaded into the trap with two-stage photoionization: neutral radium is driven to the $^1P_1$ state with near-resonant 483-nm light and then ionized with 450-nm light. Radium ions are consistently trapped within 15 min of the oven reaching the target temperature. This long-term ^{225}Ra source opens the door to working with $^{225}Ra^{+}$ ions with high duty cycles in sealed systems.

To laser cool $^{225}Ra^{+}$, we drive optical transitions from hyperfine levels of the $^2S_{1/2}$ and $^2D_{3/2}$ states to the $^2P_{1/2}$ state, see Fig. 1(a). The ions are held in a linear Paul trap with characteristic radial and axial dimensions $r_0 = 0.6$ mm and $z_0 = 2.5$ mm [17]. The radial electrodes are driven at 8.205 MHz, and dc offsets up to +200 mV and −200 mV are applied to opposite electrode pairs to break the degeneracy between radial motional modes. We can trap chains of ions, see Fig. 1(b), though measurements were performed with single ions. Four lasers address all hyperfine levels in the $^2S_{1/2}$ ground and $^2D_{3/2}$ metastable states, see Fig. 1(a). The frequency and power of each laser is independently controlled with acousto-optic modulators set up in double-pass configurations. Decays from the $^2P_{1/2}$ state populate both the ground state and the metastable $^2D_{3/2}$ state (642(9) ms lifetime [18]). The $^2D_{3/2}$ state hyperfine levels are repumped with 1079-nm light, which returns the ion to the ground state via the $D_{3/2} \leftrightarrow P_{1/2}$ transition. Both 468-nm lasers and one

*Contact author: roy.a.ready@gmail.com

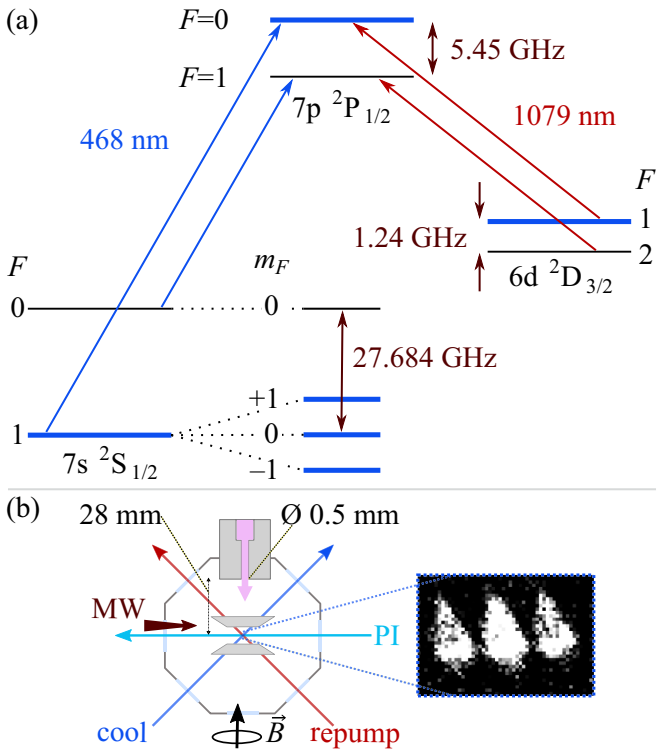

FIG. 1. (a) Energy-level diagram of the low-lying $^{225}Ra^{+}$ hyperfine structure and $^{2}S_{1/2}$ Zeeman sublevels, showing laser and microwave-driven (MW) transitions. State detection lasers drive transitions between the bright states (blue) and are off-resonant from the dark states (black). (b) Experimental apparatus. An oven emits radium atoms (pink arrow) that are photoionized by (PI) light at 483 nm and 450 nm. Trapped ions, such as the three shown, are detected and laser-cooled with light at 468 nm. Our objective introduces aberrations to the image but does not affect our measurements. Permanent magnets define the quantization axis ($\vec{B}$), and hyperfine transitions are driven by a microwave horn.

repump laser are stabilized to an optical cavity with a finesse of ≈1000 and a laser linewidth below 2 MHz. The second repump laser is offset locked [19] to its counterpart. We use the first-order sidebands of fiber electro-optic modulators (EOMs) to scan the 468-nm and 1079-nm light across the hyperfine levels and also use the 468-nm EOM for state preparation, following Olmschenk *et al.* [7].

Microwave spectroscopy of the $^{2}S_{1/2}$ state is performed with a horn positioned 10 cm from the trap center, see Fig. 1(b). The microwaves are generated by mixing a fixed tone at 27.3 GHz with a tunable rf source from a direct digital synthesizer that is frequency doubled to 385 MHz.

Each hyperfine splitting measurement consists of Doppler cooling, state preparation, driving the spectroscopy transition, and state detection. For $^{2}S_{1/2}(F=0)$ state preparation, we drive the $S_{1/2}(F=1) \leftrightarrow P_{1/2}(F=1)$ transition for 100 µs while repumping both $D_{3/2}$ hyperfine levels. During state detection, the $S_{1/2}(F=1) \leftrightarrow P_{1/2}(F=0)$ transition is driven. To prevent leakage to the $^{2}D_{3/2}$ $(F=1)$ state, we repump the population using the $D_{3/2}(F=1) \leftrightarrow P_{1/2}(F=0)$ transition. The $^{2}S_{1/2}$ $(F=1)$ and $^{2}D_{3/2}(F=1)$ states are referred to as bright states, shaded blue in Fig. 1(a). Otherwise the ion is in one of the dark states, $^{2}S_{1/2}(F=0)$ or $^{2}D_{3/2}(F=2)$, and light is not scattered as the dark states are far off resonance from the state detection lasers. Scattered 468-nm photons are focused onto a photomultiplier tube (PMT) and camera by an objective.

We characterize the hyperfine qubit by measuring the SPAM fidelity. After preparing the dark ground state, we transfer the population to the $^{2}S_{1/2}(F=1, m_F=0)$ bright state with a 235 − µs resonant microwave pulse and perform state detection. This is compared to state detection after only $^{2}S_{1/2}(F=0)$ dark-state preparation (no microwave pulse). From the SPAM measurement we find a 2.5 photon threshold to discriminate between bright events (11.6 photons on average) and dark events (0.04 photons on average) in a 1.7-ms detection time, see Fig. 2(a). The threshold minimizes the average false detection fraction, given by $1/2(\epsilon_0+\epsilon_1)$ [20], where ϵ_0 (ϵ_1) is the fraction of dark (bright) events falsely identified as bright (dark) events and is related to the fidelity by $\mathcal{F}=1-1/2(\epsilon_0+\epsilon_1)$. We determine the fidelity from an average of 13 measurements, with a single representative measurement shown in Fig. 2(a). The measured average SPAM fidelity is $\mathcal{F}=0.9951(9)$, with false identification fractions of $\epsilon_0=0.0035(8)$ and $\epsilon_1=0.007(2)$. The result is limited by off-resonant scattering, PMT dark counts, and the measured (with statistical uncertainty) 0.2241(11)% photon detection efficiency [21]. The photon detection efficiency was measured by preparing the ion into the $^{2}D_{3/2}(F=1)$ state and measuring the 468-nm photons while repumping with 1079-nm light, following Ramm *et al.* [21]. Our $^{225}Ra^{+}$ hyperfine SPAM result compares favorably to recent results in similar systems [20,22]. The fidelity can be improved with a larger numerical aperture collection objective [22] or by shelving population in the $^{2}D_{5/2}$ state with 728-nm laser light.

The $S_{1/2}(F=1, m_F=0) \leftrightarrow S_{1/2}(F=0, m_F=0)$ hyperfine transition is sensitive to the second-order Zeeman shift $\Delta\nu_{QZ}=C_2B^2$, where C_2 is the quadratic Zeeman shift coefficient and B is the magnitude of the magnetic field at the ion. We measured $\Delta\nu_{QZ}$ for different magnetic field strengths that were varied by moving a permanent magnet. The magnet field is approximately perpendicular to the trap axis, see Fig. 1. The field direction varies slightly when changing the magnet position and affects the relative coupling strength of the microwave π and $\sigma^{\pm}$ transitions. However, the line centers of the transitions are unaffected by these fluctuations and the linewidths are Fourier limited. We did not use shielding so the ambient B-field drifts over the course of a measurement. The maximum observed drift rate is 9 µG min^{-1} and does not significantly affect our results. From fitting these measurements we extract the quadratic Zeeman shift coefficient, $C_2=142.3(1.0)\ \mathrm{Hz\,G^{-2}}$, see Fig. 2(b). Our result is consistent with the calculated value of 141 $\mathrm{Hz\,G^{-2}}$ [23].

We perform interleaved Ramsey and Rabi spectroscopy sequences to measure the ground-state hyperfine splitting. First, we prepare the $^{2}S_{1/2}(F=0, m_F=0)$ state. Then we scan either two 1.8-ms $\pi/2$ microwave pulses separated by 10 ms or a single 10-ms microwave pulse across the $S_{1/2}(F=0, m_F=0) \leftrightarrow S_{1/2}(F=1, m_F=0)$ π transition. After the Ramsey or Rabi measurement, we perform state detection. To obtain the unperturbed π transition frequency,

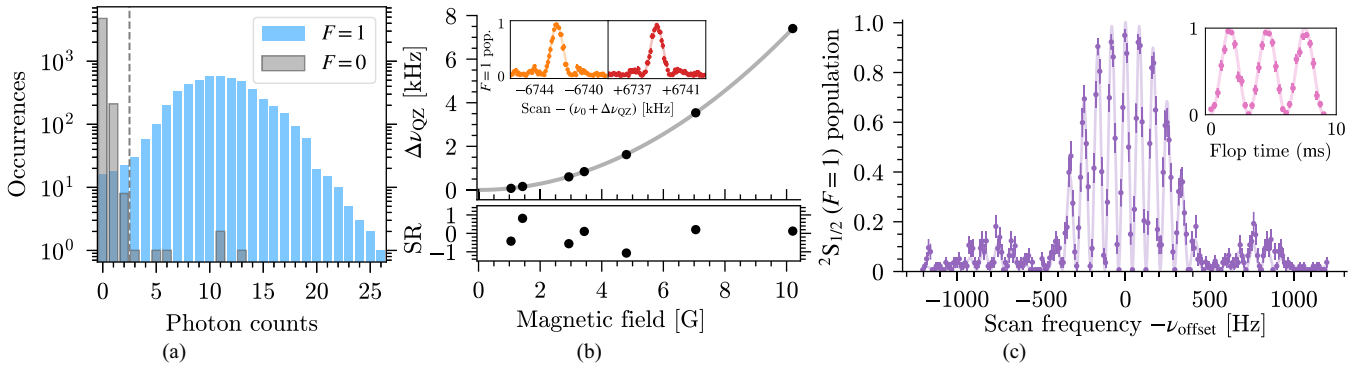

FIG. 2. (a) State preparation and measurement results for the ground-state hyperfine transition. We measure an average of 0.04 photons in the dark state and 11.6 photons in the bright state. (b) The quadratic Zeeman shift for a range of magnetic field strengths, with studentized residuals (SR) from the quadratic fit used to extract C_2, in the bottom panel. We determine the magnetic field magnitude at the ion by driving σ^+ (orange) and σ^- (red) transitions from the $m_F = \pm 1$ Zeeman levels, shown for the 1.5-G data point. (c) Spectroscopy of the $S_{1/2}(F = 1, m_F = 0) \leftrightarrow S_{1/2}(F = 0, m_F = 0)$ transition, offset by $\nu_{\text{offset}} = 276\,845\,117\,30$ Hz. A $\pi/2$ pulse time is determined from a Rabi flop, an example of which is shown (pink inset).

$\Delta\nu_{QZ}$ [$B = 2.183(3)$ G] is subtracted from the scanned frequency. We average 111 Ramsey and 10 interleaved Rabi measurements to determine the hyperfine splitting frequency, with a single representative Ramsey measurement shown in Fig. 2(c). This results in the ground-state hyperfine constant $A(S_{1/2}) = -27.684\,511\,052(5)$ GHz. The statistical uncertainty is 0.6 Hz, which is negligible compared to the 5-Hz total systematic uncertainty.

The dominant source of uncertainty of the $^2S_{1/2}$ hyperfine splitting comes from the second-order Zeeman shift, which shifts the frequency of the measured transition by $\Delta\nu_{QZ}(B)$. We measure B from the Zeeman splitting of the $(F = 0, m_F = 0) \leftrightarrow (F = 1, m_F = \pm 1)$, $\sigma^\pm$ transitions, see Fig. 2(b) inset. The average frequency of the $\sigma^\pm$ transitions is subtracted from the π transition frequency to determine $\Delta\nu_{QZ}(B)$. The uncertainties for the quadratic Zeeman shift data points are derived from fits to the transitions and contribute almost the entirety of the 5 Hz to the measured ground-state hyperfine splitting.

The second-largest contribution to the systematic uncertainty is due to the ac magnetic field B_{ac} generated by imbalanced rf currents in the trap electrodes. We measured the π transition frequency for different trap rf powers to characterize this effect. We found that the shift is consistent with zero, with $B_{ac} \leqslant 60$ mG, corresponding to a 0.5-Hz uncertainty.

The third largest contribution to the systematic uncertainty is inaccuracy of the rf source, which is locked to a GPS-disciplined reference (SRS FS740). We assign an uncertainty of 0.3 Hz to this systematic, derived from the reference 1×10^{-11} short-term stability.

We tested for ac Stark shifts from probe laser light leakage but did not observe any frequency shifts due to this effect. We also are not sensitive to shifts due to blackbody radiation, which we estimate to be below 10 μHz.

The $^2S_{1/2}$ and $^2P_{1/2}$ hyperfine splittings of $^{225}Ra^+$ were first measured by laser spectroscopy of a hot atomic beam by Ahmad *et al.* [24]. The ground-state hyperfine splitting was remeasured by Neu *et al.* [25] and resulted in a 47(26) MHz (3.6σ) discrepancy with the original measurement. Of the two previous $A(S_{1/2})$ hyperfine constant measurements, our result is in agreement with the first measurement [24], see Fig. 3.

We measured the hyperfine splittings of the $^2D_{3/2}$ and $^2P_{1/2}$ excited states with laser spectroscopy. For both excited states we scan over a transition with the first-order sideband of a fiber EOM. The 468-nm EOM sideband drives the $S_{1/2}(F = 1) \leftrightarrow P_{1/2}(F = 1)$ transition, and the 1079-nm EOM sideband drives the $D_{3/2}(F = 1) \leftrightarrow P_{1/2}(F = 1)$ transition. We reference the laser carrier frequency by performing spectroscopy on the $D_{3/2}(F = 2) \leftrightarrow P_{1/2}(F = 1)$ and the $S_{1/2}(F = 1) \leftrightarrow P_{1/2}(F = 0)$ transitions for the $^2D_{3/2}$ and $^2P_{1/2}$ hyperfine splitting measurements, respectively.

To measure the hyperfine splitting of the $^2D_{3/2}$ state, we prepare the population in the $^2D_{3/2}(F = 1)$ hyperfine level, scan the 1079-nm EOM sideband frequency, and perform state detection. The dark-state population is maximized when the EOM sideband frequency is resonant with the $^2D_{3/2}$ hyperfine splitting, see Fig. 4. The hyperfine splitting is then determined from the difference of the $D_{3/2}(F = 2) \leftrightarrow P_{1/2}(F = 1)$ and $D_{3/2}(F = 1) \leftrightarrow P_{1/2}(F = 1)$ transition frequencies. The measured hyperfine splitting is 1.239(2) GHz, which corresponds to a hyperfine constant of $A(D_{3/2}) = -619.7(1.1)$ MHz. The statistical and systematic uncertainties are 100 kHz and 1.1 MHz.

To measure the $^2P_{1/2}$ hyperfine splitting, we prepare the $^2S_{1/2}(F = 1)$ bright state, scan the 468-nm EOM sideband frequency, and perform state detection. The hyperfine splitting is determined from the frequency difference of the $S_{1/2}(F = 1) \leftrightarrow P_{1/2}(F = 0)$ and $S_{1/2}(F = 1) \leftrightarrow P_{1/2}(F = 1)$ transitions. The measured hyperfine splitting constant is $A(P_{1/2}) = -5.447(4)$ GHz. The uncertainty is dominated by the 4.0-MHz systematic uncertainty, primarily due to drift in the cavity that stabilizes the 468-nm laser. The statistical uncertainty is 120 kHz. Our result is consistent with the previous measurement [24] and improves the precision by a factor of 1.9.

The $^2P_{1/2}$ and $^2D_{3/2}$ hyperfine splitting measurements share the same sources of systematic uncertainty. The leading

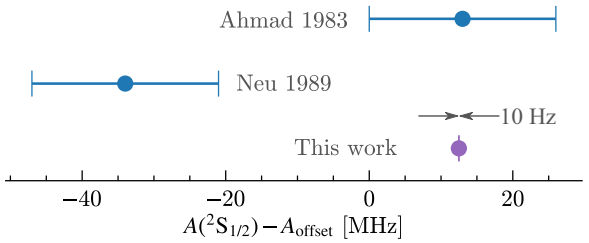

FIG. 3. A comparison of our result (purple) with previous measurements [24,25] (blue) of the $A(S_{1/2})$ hyperfine constant. The plotted values are offset by $A_{offset} = -27.704$ GHz.

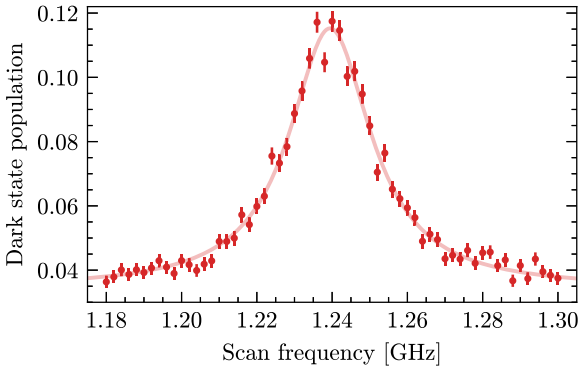

FIG. 4. The $^2S_{1/2}(F = 0)$ and $^2D_{3/2}(F = 2)$ dark-state population as the 1079-nm EOM first-order sideband is scanned over the $D_{3/2}(F = 1) \leftrightarrow P_{1/2}(F = 1)$ transition. A Lorentzian fit determines the $^2D_{3/2}$ hyperfine splitting.

source of uncertainty for both the $^2P_{1/2}$ and $^2D_{3/2}$ hyperfine measurements is drift of our laser stabilization cavities, which results in laser frequency drifts during measurements. We characterize the drift and assign uncertainties of 3.2 MHz to the $^2P_{1/2}$ and 0.7 MHz to the $^2D_{3/2}$ measurements.

The combination of Zeeman splitting with imperfect linear laser polarization or with an unequal population distribution in the Zeeman sublevels used for state preparation results in a systematic shift of the $^2P_{1/2}$ and $^2D_{3/2}$ hyperfine frequencies. For this shift we assign an uncertainty that corresponds to the largest Zeeman splitting of each transition, measured at a magnetic field of 1.1 G. The resulting uncertainty is 1.6 MHz for the $^2P_{1/2}$ measurement and 0.8 MHz for the $^2D_{3/2}$ measurement.

We investigated frequency shifts of the $^2P_{1/2}$ and $^2D_{3/2}$ states due to ac Stark effect from the probe lasers by varying the 468-nm laser power from 5.0 μW to 15.0 μW and varying the 1079-nm laser power from 1.7 μW to 11.0 μW. We did not observe ac Stark shifts for either the $^2P_{1/2}$ or $^2D_{3/2}$ measurements, which is consistent with our calculated upper bound of 10 kHz.

Hyperfine measurements allow us to indirectly study nuclear magnetization, whose contribution to the hyperfine splitting is known as the Bohr-Weisskopf (BW) effect. Direct nuclear calculations of the BW effect are challenging, with a 30% uncertainty for the $^2S_{1/2}$ state of $^{225}Ra^+$ [26]. But the effect can also be determined with a combination of atomic theory and hyperfine measurements [27]. The uncertainty from atomic theory (0.5% in Skripnikov [28] and 0.8% in Cserveny and Roberts [29]) is larger than the previous measurement uncertainty [25]. Nevertheless, our measurement combined with atomic theory shifts the BW value by several percent and reduces the uncertainty by a few tenths of a percent. As theory improves, this hyperfine measurement will be increasingly important for our understanding of nuclear physics effects. The ground-state hyperfine measurement may also be used to improve knowledge of the BW effect for $^{225}Ra^+$ excited states [27].

In summary, we have operated a $^{225}Ra^+$ ion trap for over two years in a sealed vacuum system and measured the hyperfine splitting of the states used for laser cooling and state detection. The demonstrated long-term source of short-lived radium isotopes enables the development of a $^{225}Ra^+$ ion optical clock, whose hyperfine structure is amenable to operation as a two-laser infrared clock [14]. Our SPAM result using only the three lowest electronic levels, i.e., there is no additional auxiliary shelving, and the ion's large hyperfine splitting make a case for $^{225}Ra^+$ as a system for QIS applications [30].

Tests of time-reversal symmetry with ^{225}Ra benefit from its nuclear structure, which enhances experimental sensitivity to the Schiff moment [31–33]. Sensitivity can be further enhanced by incorporating ^{225}Ra into a molecule [34], which can be synthesized with laser-cooled $^{225}Ra^+$ [17]. The hyperfine and optical qubit features of $^{225}Ra^+$ can be utilized in molecular spectroscopy techniques such as quantum logic spectroscopy [35,36]. Finally, $^{225}Ra^+$ ions are a potential route to trapped actinium ions, as ^{225}Ra beta-decays to $^{225}Ac^+$, and therefore $^{225}Ra^+$ decays could result in trapped $^{225}Ac^{2+}$, which supports laser cooling and state detection in two independent manifolds.

Acknowledgments. We thank Sam Brewer, Wes Campbell, Christian Sanner, Qiming Wu, and Anthony Ransford for helpful discussions. H.L. was supported by ONR Grant No. N00014-21-1-2597, and M.F. was supported by DOE Award No. DE-SC0022034. R.A.R., S.K., R.K., A.S., H.D., C.A.H., X.S., L.S.W., and A.M.J. were supported by Heising-Simons Foundation Award No. 2022-4066, the W.M. Keck Foundation, NIST Award No. 60NANB21D185, NSF NRT Award No. 2152201, the Eddleman Center, the Noyce Initiative, NSF Awards No. 2326810, No. 2146555, and No. 1912665, and ONR Award No. N00014-25-1-2131. A.N.G. acknowledges the support of startup funds and Michigan State University. The isotope used in this research was supplied by the U.S. Department of Energy Isotope Program, managed by the Office of Isotope R&D and Production.

Data availability. The main data supporting the findings of this Letter are openly available [37].

[1] S. Crain, E. Mount, S. Baek, and J. Kim, Individual addressing of trapped $^{171}Yb+$ ion qubits using a microelectromechanical systems-based beam steering system, Appl. Phys. Lett. **105**, 181115 (2014).

[2] N. C. Lewty, B. L. Chuah, R. Cazan, B. K. Sahoo, and M. D. Barrett, Spectroscopy on a single trapped $^{137}Ba^{+}$ ion for nuclear magnetic octupole moment determination, Opt. Express **20**, 21379 (2012).

[3] M. Pizzocaro, P. Thoumany, B. Rauf, F. Bregolin, G. Milani, C. Clivati, G. A. Costanzo, F. Levi, and D. Calonico, Absolute frequency measurement of the $^{1}S_0-^{3}P_0$ transition of ^{171}Yb, Metrologia **54**, 102 (2017).

[4] C. J. Ballance, T. P. Harty, N. M. Linke, M. A. Sepiol, and D. M. Lucas, High-fidelity quantum logic gates using trapped-ion hyperfine qubits, Phys. Rev. Lett. **117**, 060504 (2016).

[5] M. J. Boguslawski, Z. J. Wall, S. R. Vizvary, I. D. Moore, M. Bareian, D. T. C. Allcock, D. J. Wineland, E. R. Hudson, and W. C. Campbell, Raman scattering errors in stimulated-Raman-induced logic gates in $^{133}Ba^{+}$, Phys. Rev. Lett. **131**, 063001 (2023).

[6] C. Balzer, A. Braun, T. Hannemann, C. Paape, M. Ettler, W. Neuhauser, and C. Wunderlich, Electrodynamically trapped Yb^{+} ions for quantum information processing, Phys. Rev. A **73**, 041407(R) (2006).

[7] S. Olmschenk, K. C. Younge, D. L. Moehring, D. N. Matsukevich, P. Maunz, and C. Monroe, Manipulation and detection of a trapped Yb^{+} hyperfine qubit, Phys. Rev. A **76**, 052314 (2007).

[8] D. Hucul, J. E. Christensen, E. R. Hudson, and W. C. Campbell, Spectroscopy of a synthetic trapped ion qubit, Phys. Rev. Lett. **119**, 100501 (2017).

[9] C. Tamm, N. Huntemann, B. Lipphardt, V. Gerginov, N. Nemitz, M. Kazda, S. Weyers, and E. Peik, Cs-based optical frequency measurement using cross-linked optical and microwave oscillators, Phys. Rev. A **89**, 023820 (2014).

[10] N. Huntemann, C. Sanner, B. Lipphardt, C. Tamm, and E. Peik, Single-ion atomic clock with 3×10^{-18} systematic uncertainty, Phys. Rev. Lett. **116**, 063001 (2016).

[11] C. A. Holliman, M. Fan, A. Contractor, S. M. Brewer, and A. M. Jayich, Radium ion optical clock, Phys. Rev. Lett. **128**, 033202 (2022).

[12] M. Fan, C. A. Holliman, A. L. Wang, and A. M. Jayich, Laser cooling of radium ions, Phys. Rev. Lett. **122**, 223001 (2019).

[13] G. N. West, W. Loh, D. Kharas, C. Sorace-Agaskar, K. K. Mehta, J. Sage, J. Chiaverini, and R. J. Ram, Low-loss integrated photonics for the blue and ultraviolet regime, APL Photonics **4**, 026101 (2019).

[14] C. A. Holliman, M. Fan, and A. M. Jayich, Ion optical clocks with three electronic states, in *Quantum Sensing, Imaging, and Precision Metrology* (SPIE, Bellingham, WA, 2023), Vol. PC12447, p. PC124470C.

[15] M. Fan, R. A. Ready, H. Li, S. Kofford, R. Kwapisz, C. A. Holliman, M. S. Ladabaum, A. N. Gaiser, J. R. Griswold, and A. M. Jayich, Laser cooling and trapping of $^{224}Ra^{+}$, Phys. Rev. Res. **5**, 043201 (2023).

[16] R. M. Essex, J. L. Mann, R. Collé, L. Laureano-Perez, M. E. Bennett, H. Dion, R. Fitzgerald, A. M. Gaffney, A. Gourgiotis, A. Hubert, K. G. W. Inn, W. S. Kinman, S. P. Lamont, R. Steiner, and R. W. Williams, New determination of the ^{229}Th half-life, J. Radiol. Nucl. Chem. **318**, 515 (2018).

[17] M. Fan, C. A. Holliman, X. Shi, H. Zhang, M. W. Straus, X. Li, S. W. Buechele, and A. M. Jayich, Optical mass spectrometry of cold $RaOH^{+}$ and $RaOCH_3{}^{+}$, Phys. Rev. Lett. **126**, 023002 (2021).

[18] H. Li, H. Dan, M. Fan, S. Kofford, R. Kwapisz, R. A. Ready, A. Sawhney, M. Brzeczek, C. Holliman, A. M. Jayich, S. G. Porsev, and M. S. Safronova, Lifetimes of the metastable $6d\,^{2}D_{5/2}$ and $6d\,^{2}D_{3/2}$ states of Ra^{+}, Phys. Rev. Lett. **135**, 073001 (2025).

[19] U. Schünemann, H. Engler, R. Grimm, M. Weidemüller, and M. Zielonkowski, Simple scheme for tunable frequency offset locking of two lasers, Rev. Sci. Instrum. **70**, 242 (1999).

[20] J. E. Christensen, D. Hucul, W. C. Campbell, and E. R. Hudson, High-fidelity manipulation of a qubit enabled by a manufactured nucleus, npj Quantum Inf. **6**, 35 (2020).

[21] M. Ramm, T. Pruttivarasin, M. Kokish, I. Talukdar, and H. Häffner, Precision measurement method for branching fractions of excited $P_{1/2}$ states applied to $^{40}Ca^{+}$, Phys. Rev. Lett. **111**, 023004 (2013).

[22] S. Crain, C. Cahall, G. Vrijsen, E. E. Wollman, M. D. Shaw, V. B. Verma, S. W. Nam, and J. Kim, High-speed low-crosstalk detection of a $^{171}Yb+$ qubit using superconducting nanowire single photon detectors, Commun. Phys. **2**, 97 (2019).

[23] O. O. Versolato, L. W. Wansbeek, K. Jungmann, R. G. E. Timmermans, L. Willmann, and H. W. Wilschut, Potential of electric quadrupole transitions in radium isotopes for single-ion optical frequency standards, Phys. Rev. A **83**, 043829 (2011).

[24] S. A. Ahmad, W. Klempt, R. Neugart, E. W. Otten, K. Wendt, and C. Ekström, Determination of nuclear spins and moments in a series of radium isotopes, Phys. Lett. B **133**, 47 (1983).

[25] W. Neu, R. Neugart, E. W. Otten, G. Passler, K. Wendt, B. Fricke, E. Arnold, H. J. Kluge, and G. Ulm, Quadrupole moments of radium isotopes from the $7p^{2}P_{3/2}$ hyperfine structure in Ra II, Z. Phys. D **11**, 105 (1988).

[26] J. S. M. Ginges, A. V. Volotka, and S. Fritzsche, Ground-state hyperfine splitting for Rb, Cs, Fr, Ba^{+}, and Ra^{+}, Phys. Rev. A **96**, 062502 (2017).

[27] J. S. M. Ginges and A. V. Volotka, Testing atomic wave functions in the nuclear vicinity: The hyperfine structure with empirically deduced nuclear and quantum electrodynamic effects, Phys. Rev. A **98**, 032504 (2018).

[28] L. V. Skripnikov, Nuclear magnetization distribution effect in molecules: Ra+ and RaF hyperfine structure, J. Chem. Phys. **153**, 114114 (2020).

[29] R. B. Cserveny and B. M. Roberts, Theoretical characterization of the barium II and radium II ions, Phys. Rev. A **112**, 032816 (2025).

[30] C. Zhang, J. Phillips, I. Monga, E. Saglamyurek, Q. Wu, and H. Haeffner, Mitigation of birefringence in cavity-based quantum networks using frequency-encoded photons, Phys. Rev. A **111**, 062608 (2025).

[31] N. Auerbach, V. V. Flambaum, and V. Spevak, Collective T - and P-odd electromagnetic moments in nuclei with octupole deformations, Phys. Rev. Lett. **76**, 4316 (1996).

[32] J. Dobaczewski and J. Engel, Nuclear time-reversal violation and the Schiff moment of ^{225}Ra, Phys. Rev. Lett. **94**, 232502 (2005).

[33] M. Bishof, R. H. Parker, K. G. Bailey, J. P. Greene, R. J. Holt, M. R. Kalita, W. Korsch, N. D. Lemke, Z.-T. Lu, P. Mueller, T. P. O'Connor, J. T. Singh, and M. R. Dietrich, Improved limit

on the ^{225}Ra electric dipole moment, Phys. Rev. C **94**, 025501 (2016).

[34] P. Yu and N. R. Hutzler, Probing fundamental symmetries of deformed nuclei in symmetric top molecules, Phys. Rev. Lett. **126**, 023003 (2021).

[35] P. O. Schmidt, T. Rosenband, C. Langer, W. M. Itano, J. C. Bergquist, and D. J. Wineland, Spectroscopy using quantum logic, Science **309**, 749 (2005).

[36] C.-w. Chou, C. Kurz, D. B. Hume, P. N. Plessow, D. R. Leibrandt, and D. Leibfried, Preparation and coherent manipulation of pure quantum states of a single molecular ion, Nature (London) **545**, 203 (2017).

[37] R. Ready, Laser cooling and hyperfine measurements of $^{225}Ra^{+}$ ions, Version 0.1.0 [Data set], Zenodo, 2026, https://doi.org/10.5281/zenodo.20801476.